

Journal of Materials Chemistry B

Accepted Manuscript



This is an *Accepted Manuscript*, which has been through the Royal Society of Chemistry peer review process and has been accepted for publication.

Accepted Manuscripts are published online shortly after acceptance, before technical editing, formatting and proof reading. Using this free service, authors can make their results available to the community, in citable form, before we publish the edited article. We will replace this *Accepted Manuscript* with the edited and formatted *Advance Article* as soon as it is available.

You can find more information about *Accepted Manuscripts* in the [Information for Authors](#).

Please note that technical editing may introduce minor changes to the text and/or graphics, which may alter content. The journal's standard [Terms & Conditions](#) and the [Ethical guidelines](#) still apply. In no event shall the Royal Society of Chemistry be held responsible for any errors or omissions in this *Accepted Manuscript* or any consequences arising from the use of any information it contains.



Journal Name

ARTICLE

Multiple noncovalent interactions mediated one-pot therapeutic assemblies for effective treatment of atherosclerosis

Yin Dou^{a,b,1}, Xiangjun Zhang^{a,1}, Xiaoqiu Xu^a, Xing Zhou^a, Songling Han^a, Ruibing Wang^c, Min Su^{a,*}, Xiaohui Li^{b,*}, Jianxiang Zhang^{a,*}

Received 00th January 20xx,
Accepted 00th January 20xx

DOI: 10.1039/x0xx00000x

www.rsc.org/

Atherosclerosis may cause life-threatening coronary artery disease, carotid artery disease, stroke, and peripheral vascular disease, while its effective therapy remains challenging thus far. With the aim to facilitate construction of efficacious and translational oral delivery systems for an anti-atherosclerotic drug of rapamycin (RAP), an all-in-one approach was created. This strategy involves a carboxyl-bearing compound (serves as a guest molecule) mediated self-assembly of a structurally simple host polymer of poly(N-isopropylacrylamide) (PNIPAm). The formation of microspheres and highly efficient packaging of RAP could be simultaneously achieved by this host-guest self-assembly, affording cost-effective therapeutic assemblies with particularly robust drug loading capacity, desirable drug dissolution, relative manufacturing simplicity, good lyophilization-reconstitution character, and facile scalability. Besides these pharmaceutical characteristics superior over control microspheres based on poly(lactide-co-glycolide) or an enteric coating material, therapeutic RAP microspheres fabricated by this assembly approach had high oral bioavailability. More importantly, assembled RAP microspheres displayed significant therapeutic advantages upon treatment of atherosclerosis in an apolipoprotein E-deficient mouse model. In addition, long-term treatment with either RAP-containing assemblies or the carrier material PNIPAm revealed a good safety profile in mice post oral delivery. Accordingly, RAP microspheres developed herein are promising and translational therapeutics for atherosclerotic diseases. This study also provides new insights into the design of effective carrier materials for various lipophilic therapeutics.

Introduction

Cardiovascular disease remains the leading cause of morbidity and mortality in developed countries, and likely soon become the preeminent health problem worldwide.^{1,2} Atherosclerosis, a chronic inflammatory process characterized by the formation of atheromatous plaques in the intima of medium- and large-sized arteries, may cause life-threatening coronary artery disease, carotid artery disease, stroke, and peripheral vascular disease.^{1, 3, 4} Pharmaceutical treatment is an effective strategy for the management of atherosclerosis.⁵⁻⁸ Rapamycin (RAP), a potent immunosuppressant and an inhibitor of the mammalian target of rapamycin (mTOR) pathway, has been considered to be an effective anti-atherosclerotic agent, in view of its multiple pharmacological activities including anti-inflammation, anti-migration, anti-proliferation, and autophagy activation.⁹⁻¹⁴ Also, increasing evidence suggests that RAP is efficacious for molecularly targeted

cancer therapy, lifespan extension, Alzheimer's disease, and muscular dystrophy.¹⁵

Unfortunately, as a biopharmaceutics classification system (BCS) class II drug,¹⁶ RAP is practically insoluble in water, and its solubility in water was determined to be 2.6 µg/mL.¹⁷ Due to its poor water and oil solubility as well as low oral bioavailability,¹⁸ only few formulations of RAP have proven satisfactory for oral delivery. Therefore, different pharmaceutical strategies have been explored to address this limitation for diverse purposes. Besides drug eluting stents that have been extensively employed for the treatment of coronary artery disease,^{9,10} some other advanced delivery systems were investigated for RAP. These new platforms involve cyclodextrin inclusions,^{19,20} liposomes,²¹ polymeric nanoparticles,²²⁻²⁴ micelles,^{19, 25, 26} microparticles,^{27, 28} and RAP-polymer conjugates,²⁹ in which RAP is either physically packaged or covalently conjugated. However, these studies were largely focused on purely increasing solubility, tumor therapy, or immunosuppression, and the majority of them were only subjected to *in vitro* evaluations. Even for some *in vivo* studies, only short-term treatment was conducted post parenteral administration. Both efficacy and safety profiles remain unclear upon long-term use of these systems, particularly for formulations delivered by the intravenous route. For chronic disease, as in the case of atherosclerotic complications, long-term treatment is necessary for therapeutic intervention, which necessitates repeated dosing over a

^a Department of Pharmaceutics, College of Pharmacy, Third Military Medical University, Chongqing 400038, China.

^b Institute of Materia Medica, College of Pharmacy, Third Military Medical University, Chongqing 400038, China.

^c State Key Laboratory of Quality Research in Chinese Medicine, Institute of Chinese Medical Sciences, University of Macau, Taipa, Macau.

¹ These authors contributed equally.

Electronic Supplementary Information (ESI) available: Table S1 and Figure S1-4. See DOI: 10.1039/x0xx00000x

long period of time.³⁰ In this context, oral administration is the most desirable delivery route, in view of its advantages such as convenience, relatively good safety profile, high patient compliance, and easy modulation on dosing. To the best of our knowledge, no effective oral delivery systems of RAP have been developed so far for the long-term treatment of atherosclerosis.

With the aim to address above issues and construct effective and translational platforms for oral delivery of RAP, herein an all-in-one approach was developed. This was achieved by a carboxyl-bearing compound (CBC) mediated self-assembly of a host polymer. Through this facile but robust one-pot host-guest assembly, formation of microspheres and RAP loading could be simultaneously attained, leading to therapeutic assemblies with excellent physicochemical characters, pharmaceutical properties, and superior efficacy in a mouse model of experimental atherosclerosis.

Experimental

Materials

Azodiisobutyronitrile (AIBN), N-isopropylacrylamide (NIPAm), indomethacin (IND), sulindac (SUL), and Oil-Red O (ORO) were obtained from Sigma-Aldrich (USA). Poly(lactide-co-glycolide) (50:50, PLGA) with intrinsic viscosity of 0.50-0.65 was purchased from Polysciences, Inc (USA). Eudragit® S 100 (S100) was kindly supplied by Evonik Industries (Germany). Poly(vinyl alcohol) (PVA) (88 mol.% hydrolyzed, Mw = 25 kDa) was obtained from Acro Organics. Rapamycin (RAP) and ascomycin was purchased from Beijing Huamaik Biotechnology Co., Ltd (Beijing, China). All the other reagents are commercially available and used as received.

Synthesis of PNIPAm

Poly(N-isopropylacrylamide) (PNIPAm) was synthesized by free radical polymerization in anhydrous methanol using AIBN as an initiator.³¹ The molar ratio of NIPAm/AIBN was 50:1. PNIPAm was collected by precipitation from diethyl ether, purified by dialysis against deionized water, and then lyophilized to afford a white powder. Molecular weight (Mw) of PNIPAm was determined by gel permeation chromatography (GPC), using a Waters model 1515, equipped with a Waters 2414 refractive index detector. Tetrahydrofuran (THF) was used as the mobile phase at a flow rate of 1.0 mL/min, and Mw calibration was performed with polystyrene standards.

Preparation of Various Assemblies

A dialysis procedure was performed to fabricate various assemblies. Briefly, CBC (IND or SUL), RAP, and PNIPAm were co-dissolved in a common solvent dimethyl sulfoxide (DMSO) at different feeding ratios. The obtained solution was dialyzed against deionized water at 25°C. The polymer concentration was maintained at 10 mg/mL. The outer aqueous solution was exchanged every 2 h. After 24 h of dialysis, samples were collected for analysis without further treatment. According to these procedures, RAP-loaded

microspheres based on assemblies of IND/PNIPAm and SUL/PNIPAm were produced. The drug content of RAP in the lyophilized samples was quantified by high-performance liquid chromatography (HPLC).

Molecular Dynamics Simulation of Assembly of RAP/IND/PNIPAm

The conformation of PNIPAm was built in a three-dimensional (3D) coordinate using a Molecular Operating Environment software package builder tool (MOE's, Chemical Computing Group, Canada).³² The polymer chain was built with a head-to-tail connection with 50 structural units. PNIPAm with 5 repeating units was used as a short-chain polymer to simulate PNIPAm-PNIPAm intermolecular interactions in the docking process. The 3D structures of IND, RAP, PNIPAm, and water molecules were pre-optimized before running simulations using an all-atom MMFF94x force field with no constraints. Subsequently, the structurally pre-optimized IND, RAP, PNIPAm with 5 repeating units, and water molecules were docked into the minimized and hydrated polymer structure using an AutoDock software package (AutoDock4.2, the Scripps Research Institute) to estimate the values of binding energy and intermolecular energies.^{32,33}

For all docking calculations, the grid size was set at 126×126×126 Å using grid spaces at 0.375. To compare the values of binding energy, four search algorithms (including GA, Genetic Algorithm; LGA, Lamarckian Genetic Algorithm; SA, Simulating Annealing; and LA, Local Algorithm) built in Autodock4.2 were examined to find the most favorable geometry of drug-polymer complex. It was found that LGA predicted the strongest affinity between PNIPAm and small molecules (Table S1). For all simulations, docking runs were set to 100, while the other docking parameters were default values for all algorithms. Since the binding sites within PNIPAm are not defined, the blind docking was applied to the entire polymer chain and small molecules examined. The docking results were analyzed by Autodock tools (ADT 1.56). PNIPAm-PNIPAm interactions were estimated by docking a short chain PNIPAm to PNIPAm, and calculated by the units with the highest interaction energy.

To interrogate the effects of PNIPAm conformation on IND-PNIPAm and RAP-PNIPAm interactions, IND-docked PNIPAm with the lowest energy conformation was acquired, which was employed as the host for docking with RAP to achieve the lowest energy conformation for IND-RAP. Then PNIPAm and IND-RAP were utilized to perform molecular dynamics (MD) simulations in water environment, using a canonical ensemble with an integration time step of 1 fs and a total simulation time of 5 ns, at a target temperature of 300 K.

Preparation of Drug-Loaded Microparticles by an Emulsion Technique

RAP-containing microparticles based on either PLGA or S100 were fabricated by an oil-in-water (o/w) emulsion solvent evaporation technique.³⁴ To prepare PLGA microparticles, both polymer and drug were dissolved in dichloromethane (DCM) to attain an oil phase, while 2 wt.% PVA in aqueous solution was employed as a water phase. An o/w emulsion was obtained by homogenization at

25000 rpm. The solidified microspheres were collected by centrifugation, and rinsed four times with deionized water. RAP-loaded S100 microspheres were produced by similar procedures. In this case, the oil phase was obtained by dissolving both S100 and RAP in ethanol/DCM mixture (v:v = 1:3).

Characterization of Microparticles

Particle size and ζ -potential measurements were conducted by dynamic light scattering (DLS) on a Malvern Zetasizer Nano ZS instrument at 25°C. Transmission electron microscopy (TEM) observation was carried out on a TECNAI-10 microscope (Phillips, Netherlands) operating at an acceleration voltage of 80 kV. Scanning electron microscopy (SEM) images were taken on a field emission scanning electron microscope (XL30FEG, Phillips). Differential scanning calorimetry (DSC) was measured on a TA2000 calorimeter. DSC curves were obtained from the first heating run at a rate of 10°C min⁻¹ under a nitrogen flow of 50 mL/min. Confocal laser scanning microscopy (CLSM) observation was performed by a fluorescence microscope (Leica, Heidelberg, Germany).

In Vitro Release Study

For *in vitro* release tests, 10 mg of lyophilized samples was dispersed into 30 mL PBS (0.01 M, pH 7.4) and incubated at 37°C. At predetermined time intervals, 4.0 mL of the release medium was withdrawn, and fresh PBS was replenished. The RAP concentration in the release buffer was quantified by HPLC.

Animals

All the animal care and experimental protocols were performed in accordance with the Animal Management Rules of the Ministry of Health of the People's Republic of China (No. 55, 2001) and the guidelines for the Care and Use of Laboratory Animals of Third Military Medical University. Male Sprague Dawley (SD) rats (200–250 g) and Kunming mice (20–25 g) were obtained from the Animal Center of the Third Military Medical University, while male apolipoprotein E deficient (ApoE^{-/-}) mice (20–25 g) at 8 weeks of age were supplied by the Peking University Health Science Center (Beijing, China). Animals were housed in standard rat/mouse cages under conditions of optimum light (12:12 h light-dark cycle), temperature (22 ± 1°C), and humidity (50–60%), with *ad libitum* access to water and food. All the animals were acclimatized to the laboratory for at least 3 days before experiments.

In Vivo Pharmacokinetic Study

To investigate *in vivo* pharmacokinetic performance of RAP, 20 male SD rats were randomly assigned into four groups (n = 5), which were orally administered via gastric gavage with microparticles of RAP/PLGA, RAP/S100, RAP/IND/PNIPAm, and RAP/SUL/PNIPAm at the RAP dose of 3 mg/kg, respectively. Before administration, all animals were fasted overnight. Post delivery, blood samples were collected at predetermined time points. Subsequently, 100 μ L of the whole-blood sample and 100 μ L of internal standard solution (20 ng/mL of ascomycin in methanol) were vortex-mixed. After 500 μ L of zinc sulfate solution (50 mg/mL) and 500 μ L of acetone were

added, the obtained solution was mixed by vortex for 5 min and centrifuged at 12,000 rpm for 5 min. Then, the solvent layer was withdrawn, into which 100 μ L of NaOH aqueous solution (100 mmol/L) and 2 mL 1-chlorobutane were added, followed by vortex-mixing. After centrifugation at 2,600 rpm for 5 min, the solvent layer was collected and evaporated to dryness. The dried extracts were reconstituted with 200 μ L of the mobile phase (methanol: water = 6:4). RAP concentration was quantified by liquid chromatography-mass spectrometry. The area under the plasma drug concentration-time curve (AUC) values were calculated based on a non-compartmental model using a software of DAS 3.1.0.

Treatment of Atherosclerosis in ApoE^{-/-} Mice

Male ApoE^{-/-} mice were fed normal diet containing 0.25 wt.% cholesterol and 5 wt.% lard for three months. After the first month of Western diet, fifty mice were randomized into five groups (n = 10), which were subjected to oral administration of various formulations every three days for additional two months. One group treated with saline served as the control, while other four groups were administered with microparticles of RAP/PLGA, RAP/S100, RAP/IND/PNIPAm, and RAP/SUL/PNIPAm at the RAP dose of 3 mg/kg, respectively. During the treatment, changes in the body weight of mice were monitored. At the end of treatment, mice were sacrificed after anesthesia. The blood, whole aorta, aortic sinus, and main organs were harvested to assess the degree of atherosclerosis and possible adverse effects.

Quantification of Atherosclerotic Plaques

After ApoE^{-/-} mice were sacrificed, the extent of pathological changes was quantified by measuring the lesion area of aortas from the heart to the iliac bifurcation. Briefly, the aorta was fixed by perfusion with formalin (10 wt.% in PBS) for 50 min. After the periaortic tissue was cleaned, the aorta was opened longitudinally and stained with ORO to evaluate the plaque area. To assess the degree of atherosclerosis at the aortic origin, tissues embedded in the Tissue-Tek[®] OCT[™] compound (Sakura Finetek Inc., USA) were cross-sectioned serially at 8- μ m intervals and stained by ORO to quantify the area of atheromatous plaques. Quantitative analysis was carried out with Nis-Elements BR 3.2 software (Nikon, Japan).

Histology and Immunohistochemistry Analyses on Atherosclerotic Plaques

The aortic sinus was fixed in 10 wt.% formalin for 50 min, and then it was embedded in paraffin and cut into sections. The 6- μ m sections were stained with hematoxylin and eosin (H&E) for histopathological analysis. The content of collagen was detected by Masson's trichrome staining. For immunohistochemistry, 4- μ m sections were deparaffinized, and dried at 60°C. Endogenous peroxidase activity was inhibited with 3 wt.% hydrogen peroxide and methanol for 20 min. Subsequently, sections were blocked in 1.0 wt.% bovine serum albumin in PBS containing 0.3 wt.% Triton X-100 for 60 min. Incubation with antibodies of CD68 (for macrophage staining) and matrix metalloproteinase-9 (for MMP-9 staining) was then performed overnight. Quantitative analysis was carried out with Nis-Elements BR 3.2 software (Nikon, Japan).

Complete Blood Counts and Clinical Chemistries

Blood samples were collected into EDTA spray-coated tubes, and immediately analyzed for hematological parameters such as red blood cell (RBC), white blood cell (WBC), platelet (PLT), and hemoglobin (HGB) (Sysmex KX-21, Sysmex Co., Japan). The plasma concentrations of alanine aminotransferase (ALT), aspartate aminotransferase (AST), creatinine (CREA), and blood urea nitrogen (UREA) were also quantified (Roche Cobas C501, Roche Co., Switzerland).

Lipid and Lipoprotein Analyses

The levels of serum lipids including triglyceride (TG), total cholesterol (TCH), low-density lipoprotein (LDL), and high-density lipoprotein (HDL) were detected by an AU-2700 automatic biochemical analyzer (Olympus, Japan). The detection kits were purchased from Medical Co. Ltd (Kang Taik, Beijing), while the standard serum sample was supplied by Randox Laboratories Ltd (Northern Ireland, UK).

Determination of Serum Cytokines

Quantibody[®] Mouse Inflammation Antibody Array 1 (Raybiotech Inc, USA) was used to detect the levels of various cytokines including interferon- γ (INF- γ), interleukin-1 α (IL-1 α), interleukin-1 β (IL-1 β), interleukin-6 (IL-6), and tumor necrosis factor- α (TNF- α) according to the manufacturer's protocols. Briefly, all arrays were blocked and incubated with 100 μ L of serum at 4 $^{\circ}$ C overnight, followed by incubation with detection antibodies for 1.5 h, and then with Cy3-labeled streptavidin for 1.5 h. The chip was then exposed to a laser scanner (Axon GenePix). Quantitative array analysis was performed using the GenePix 4000B and Raybio QAM-INF-1 data processing software.

Preliminary Safety Evaluation of PNIPAm for Oral Delivery

Preliminary chronic toxicity evaluation was performed for PNIPAm in mice. PNIPAm in saline was orally administered every four days for 6 months at doses varying from 0, 125, 250, 500, to 1000 mg/kg (n = 10 in each group). Post administration, the body weight and behaviours of all animals were monitored. After 6 months, mice were sacrificed and organs including heart, liver, spleen, lung, and kidney were resected for histopathological sections by standard H&E staining. Blood samples were collected for quantification of hematological parameters and biochemical markers relevant to liver/kidney functions.

Statistical Analysis

Statistical analysis was performed by the software of PASS 13.0 using one-way ANOVA test for experiments consisting of more than two groups, and with a two-tailed, unpaired t-test in experiments with two groups. Statistical significance was assessed at $p < 0.05$.

Results and discussion

One-Pot Assembly of Microspheres for RAP Delivery

Generally, an emulsion method is adopted to package hydrophobic therapeutics into microparticles of biodegradable polymers.^{35, 36} Nevertheless, this technique does not afford high drug loadings for most drugs, since drug crystals may be formed during the solvent evaporation process as the theoretical drug feeding is relatively high, particularly when the involved drug is prone to crystallization. This is largely resulted from the relatively weak interactions between drug molecules and polymer chains, which cannot conquer forces among drug molecules that dominate crystallization.³⁷ In addition, microparticles based on this approach tend to aggregation after freeze-drying, and frequently it is difficult to achieve good reconstitution. Therefore, there is an existing and continual need for creative encapsulation strategies to address these limitations. Most recently, we found that well-defined spherical microparticles may be formed by carboxyl-bearing compound (CBC)-mediated one-pot assembly of PNIPAm through a host-guest recognition.³⁸ Moreover, hydrophobic compounds without carboxyl can also be loaded into this type of host-guest assemblies. Since microparticles formation and therapeutic packaging can be simultaneously achieved, this guest-host assembly generally renders highly effective drug loading. Accordingly, it is a particularly facile yet efficient approach to create microparticulate delivery systems for both carboxyl-containing and carboxyl-deficient lipophilic drugs, which have the potential of rescuing otherwise undeliverable drugs (Figure 1A).

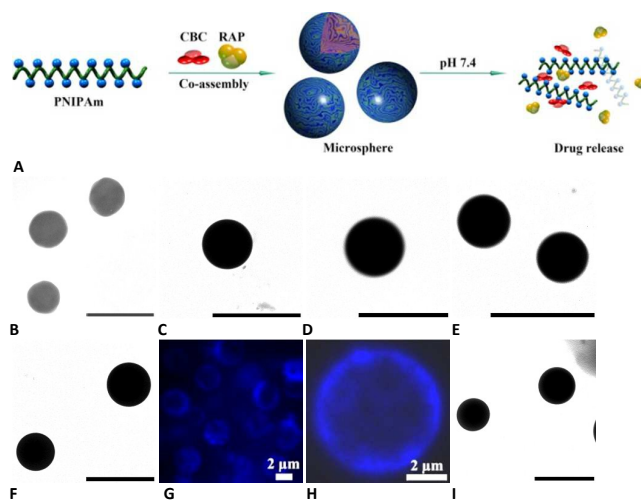


Figure 1. Host-guest assembly of RAP-containing microspheres. **A**, Schematic illustration of the host-guest assembly approach. PNIPAm, poly(N-isopropylacrylamide); CBC, carboxyl-bearing compound; RAP, rapamycin. **B-F**, TEM images of RAP-containing microspheres fabricated by host-guest assembly with IND/PNIPAm at RAP/IND/PNIPAm weight ratios of 0:2:1 (B), 0.25:2:1 (C), 0.5:2:1 (D), 1:2:1 (E), and 2:2:1 (F). **G-I**, High-magnification TEM images of microspheres at ratios 0.25:2:1 (G), 0.5:2:1 (H), and 1:2:1 (I). Scale bars are 2 μ m.

1:2:1 (E), and 2:2:1 (F). **G-H**, CLSM images of RAP-containing assemblies at the RAP/IND/PNIPAm ratio of 2:2:1. **I**, The TEM image of RAP/SUL/PNIPAm assemblies at 2:2:1. For all TEM images, scale bars represent 1 μm .

Herein, we interrogated whether CBC/PNIPAm can co-assemble with RAP and afford assemblies with effective RAP loadings, and whether the assembled RAP therapeutics can efficaciously treat atherosclerosis. For these purposes, IND and SUL were used as model CBCs, since both of them are clinically used drugs and their safety for *in vivo* applications have been fully demonstrated. On the other hand, PNIPAm with Mw of 10 kDa was employed as the guest carrier material. Co-assembly of RAP and CBC/PNIPAm was conducted by dialysis. Figure 1B-F shows TEM images of RAP-containing microspheres that were co-assembled with IND and PNIPAm using DMSO as a common solvent. Regardless of various RAP feedings, well-defined spherical assemblies could be observed. Compared with IND/PNIPAm assemblies, incorporation of RAP increased the average size of host-guest microspheres. Quantification by DLS indicated that microspheres with average size of 584, 769, 784, 737, and 614 nm were formed at RAP/IND/PNIPAm weight ratios of 0.2:1, 0.25:2:1, 0.5:2:1, 1:2:1, and 2:2:1, respectively (Figure 2A). RAP/IND/PNIPAm assemblies were further characterized by CLSM, taking advantages of the intrinsic fluorescence of IND. Whereas TEM images implied RAP/IND/PNIPAm assemblies were solid microspheres at various component ratios, CLSM revealed a vesicle-like structure for RAP/IND/PNIPAm assemblies at 2:2:1 (Figure 1G-H). This indicated that IND molecules were largely distributed in the periphery of assembled RAP/IND/PNIPAm particles. Likewise, effective formation of spherical RAP assemblies were realized when SUL/PNIPAm was utilized (Figure 1I). Consequently, these results demonstrated that RAP can co-assemble with CBC/PNIPAm to form microspheres.

Molecular Dynamics Modelling of RAP/IND/PNIPAm Assembly

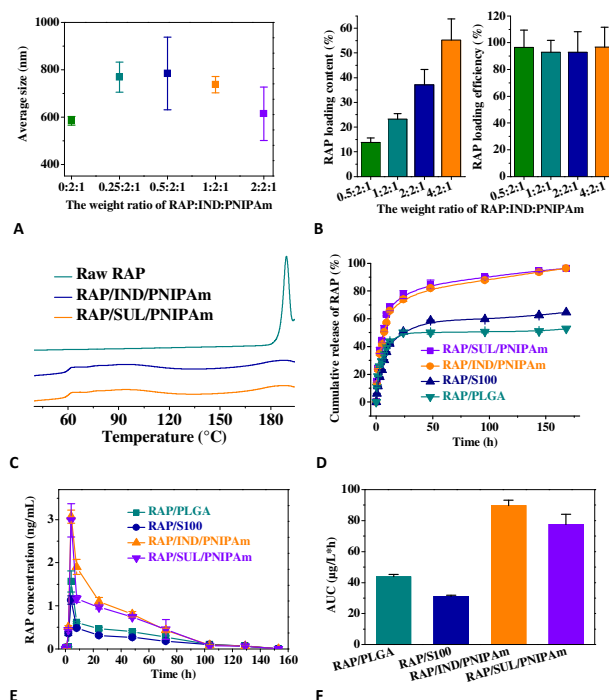


Figure 2. Physicochemical characterization and pharmacokinetic behaviours of RAP-loaded PNIPAm assemblies. **A**, The average size of PNIPAm assemblies with various contents of RAP. **B**, The effects of drug feedings on the loading content and loading efficiency of RAP in assemblies. **C**, DSC curves of raw RAP and RAP-containing microsphere derived from PNIPAm assembly. All assemblies were produced at a weight ratio 2:2:1 for RAP/IND/PNIPAm and RAP/SUL/PNIPAm. **D**, *In vitro* release profiles of various microparticles containing RAP. **E-F**, *In vivo* pharmacokinetic profiles (E) and mean AUC values (F) of various microspheres. Data are mean \pm S.D. (n = 5).

To provide additional information for co-assembly of RAP with CBC/PNIPAm, a molecular simulation approach was used, with RAP/IND/PNIPAm as a model system. We speculated that formation of RAP assemblies is driven by synergistic action of intermolecular forces among the three components that are stronger than interactions governing drug crystallization. Firstly, we estimated the values of binding energy and intermolecular energy between two components in the assembly system consisted of RAP, IND, PNIPAm, and water molecules. The magnitude of binding energy is generally used to measure the intermolecular affinity. The docking results suggest that PNIPAm displays relatively stronger affinity to both IND and RAP (Figure S1). Of note, the binding energy of IND-PNIPAm and RAP-PNIPAm is higher than that of IND-IND and RAP-RAP, respectively. In addition, considerable binding energy was

found between IND and RAP. This implied that PNIPAm can effectively interact with both IND and RAP in the three-component system of RAP/IND/PNIPAm.

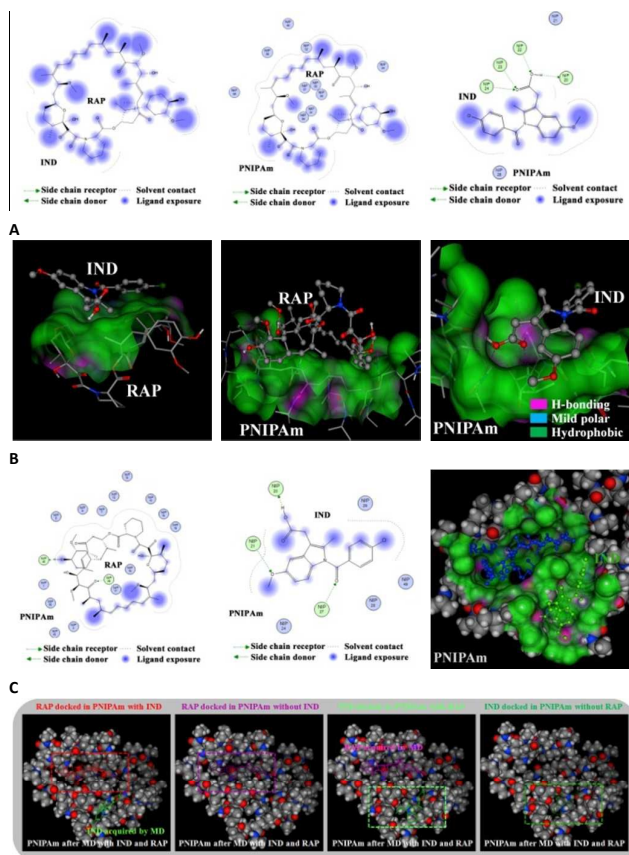


Figure 3. Molecular dynamics simulation of RAP/IND/PNIPAm assembly. **A-B**, 2D (A) and 3D (B) images showing the lowest energy conformations of IND/RAP, RAP/PNIPAm, and RAP/PNIPAm complexes. **C**, 2D and 3D conformations of the RAP/IND/PNIPAm complex after a MD stimulation. **D**, 3D conformations of RAP and IND docked in various PNIPAm complexes. In all images, colours of gray, red, and dark blue denote carbon, oxygen, and nitrogen atoms, respectively, while the light gray indicates polar hydrogen atoms that can form H-bonding. The interaction and lipophilic sites on the illustrated surface were rendered and coloured by the Connolly method built in MOE.

Figure 3A-B shows 2D and 3D images of the lowest energy complexes of IND/RAP, RAP/PNIPAm, and IND/PNIPAm, and the intermolecular energy was calculated. It was found that interactions between RAP and IND or PNIPAm are mainly composed of van der Waals and hydrophobic forces. By contrast, electrostatic, hydrophobic, and hydrogen-bonding (H-bonding) forces accounted for IND-PNIPAm interactions. Of note, the energy of either hydrophobic or H-bonding forces between IND and PNIPAm is higher than that of IND-IND and IND-RAP. Consequently, we hypothesized that PNIPAm may firstly interact with both RAP and IND through multiple interactions, and then additional IND or RAP molecules will be bound to accommodate more guest molecules. To demonstrate this hypothesis, RAP, IND, and PNIPAm were sequentially docked as a RAP/IND/PNIPAm complex to conduct a

MD simulation in water environment. We found that the RAP/IND/PNIPAm complex can be stabilized in the simulated water environment, in which RAP and IND simultaneously bound with PNIPAm to give rise to a complex structure (Figure 3C). Besides, the PNIPAm conformation obtained after the MD simulation was utilized to perform docking with IND, RAP, water, and PNIPAm. As expected, H-bonding and total intermolecular forces as well as the binding energy of RAP-PNIPAm and IND-PNIPAm are remarkably increased (Figure S1). In particular, in contrast to the neglectable H-bonding before the MD modelling, much stronger H-bonding between RAP and PNIPAm appeared after this simulation. This suggested that RAP-PNIPAm and IND-PNIPAm interactions can be dramatically enhanced during the assembly process, by modulating PNIPAm to a more comfortable conformation as compared to the initially minimized conformation.

Subsequently, the RAP/IND/PNIPAm complex was further divided into two complexes, i.e. RAP/PNIPAm and IND/PNIPAm. After their conformations were acquired by the MD simulation, RAP and IND was separately docked with them. Regardless of the presence or absence of IND, RAP shows a good affinity to the same site in the PNIPAm conformation obtained post the MD simulation (Figure 3D and Figure S2). Moreover, the total binding energy of RAP-PNIPAm or IND/PNIPAm is enhanced after the MD modelling of IND/PNIPAm or RAP/PNIPAm, respectively (Figure S2). Consequently, interactions between PNIPAm and one guest molecule may be strengthened by another guest molecule in the three-component assembly system. In other words, the presence of one guest molecule is beneficial for effective binding of the other guest molecule with the host PNIPAm.

Taken in combination, successful assembly of RAP/IND/PNIPAm and formation of RAP microspheres can be attributed to the synergistically functioned multiple interactions among the three components, which include H-bonding, hydrophobic, and van der Waals forces. While PNIPAm can effectively complex with both RAP and IND, the presence of IND benefits to a better binding of RAP with PNIPAm by modulating the configuration of PNIPAm to a more desirable one.

Effective Loading of RAP in Assembled Microspheres

Of note, effective loading of RAP into PNIPAm assemblies could be realized at various formulations examined. Quantification of the RAP content in IND/PNIPAm assemblies revealed its efficient loading, with the efficiency higher than 90% (Figure 2B). In addition, the RAP loading content was linearly enhanced when the theoretical feeding was increased, and the highest loading content of nearly 60% could be attained. Besides, DSC measurements indicated that RAP was molecularly dispersed in these assemblies (Figure 2C), which is beneficial to its dissolution, whereby enhancing bioavailability. To effectively incorporate a hydrophobic drug into microspheres, non-covalent interactions between the drug molecule and the carrier material must be strong enough to overcome drug-drug interactions that may lead to drug crystallization. This requires good compatibility between the drug and the carrier material. In the case of assembled RAP

microspheres, RAP was essentially entrapped in CBC/PNIPAm assemblies that were mediated by multiple interactions including H-bonding, hydrophobic, and electrostatic forces.³⁸ It should be emphasized that microspheres formation and RAP loading can be only achieved by assembly in deionized water or in buffers with low pH values, since CBC (with pKa of ~4.5) has extremely low solubility in these cases,^{37, 39} which may facilitate its interactions with PNIPAm while simultaneously reduce dissolution.

For comparison, PLGA (a U.S. Food and Drug Administration (FDA)-approved hydrophobic and biodegradable polymer) and S100 (a FDA approved pharmaceutical additive practically used for enteric coating formulations) were separately used as carrier materials to prepare RAP-loaded microspheres by a emulsion-based method. Although microspheres with comparable size could be produced (Figure S3), PLGA and S100 microspheres afforded the highest RAP content of about 18.1% and 17.2 (corresponding to the theoretical value of 20%), respectively. Further increment in the theoretical drug feeding led to RAP crystallization. Consequently, the host-guest assembly is a more effective approach to package RAP into microparticles. According to previous studies, H-bonding is a major force responsible for drug crystallization.⁴⁰ The host-guest system of IND/PNIPAm or SUL/PNIPAm may provide efficient H-bonding through their polar moieties of carboxyl and amide. Additional interactions such as van der Waals and hydrophobic forces as well as π - π stacking effects among aryl groups (in IND or SUL) and conjugated double bonds (in RAP) all should have contributed to successful assembly and effective loading of RAP in host-guest microspheres.

Besides highly efficient drug loading capability, the assembled microspheres exhibited excellent freeze-drying/reconstitution character. By contrast, significant aggregation occurred for lyophilized PLGA or S100 microparticles based on the emulsion method, which were extremely difficult to achieve desirable re-dispersion in aqueous solution. Moreover, this assembly approach can be easily scaled up. For RAP microspheres, tens to hundreds of grams of assemblies could be conveniently obtained in the laboratory with excellent repeatability. Also, PNIPAm is a cost-effective material that can be conveniently synthesized with delicately controlled molecular weight and well-tailored structure. All these attributes make assembled RAP microspheres attractive from the view point of bench-to-bedside translation.

***In Vitro* Release and *In Vivo* Pharmacokinetic Studies**

In vitro release study was then performed in PBS at pH 7.4. As illustrated in Figure 2D, rapid RAP release could be observed for both assembled RAP microspheres. Within 24 h, 74.0% and 77.4% of total RAP was released from RAP/IND/PNIPAm and RAP/SUL/PNIPAm, respectively. By contrast, PLGA and S100 microspheres showed a cumulative release of 50.1% and 51.0% at 24 h, respectively. On the one hand, the relative hydrophilic nature of PNIPAm should be responsible for the rapid release of RAP from assembled microspheres. On the other hand, IND or SUL molecules in RAP assemblies will dissociate in PBS at pH 7.4 that is higher than their pKa value of ~4.5,⁴¹ which may dramatically enhance their

solubility and lead to disintegration of assembled microspheres, thereby accelerating RAP dissolution. Besides, the amorphous state of RAP, as evidenced by DSC measurement (Figure 2C), was beneficial for its release.

In vivo pharmacokinetic experiments offered results well agreeing with *in vitro* release profiles. After oral administration in rats, assembled RAP microspheres displayed significantly higher blood concentrations of RAP at each time point, as compared to either PLGA or S100 microparticles (Figure 2E). Based on these data, a simple calculation showed AUC of the RAP microsphere based on IND/PNIPAm assembly was 2.0 and 2.9 times of that derived from PLGA and S100, respectively, while RAP/SUL/PNIPAm showed 1.8 and 2.5-fold of AUC when separately compared with the RAP/PLGA and RAP/S100 microsphere (Figure 2F). As a consequence, the oral bioavailability of RAP could be prominently enhanced, by incorporating it into microspheres based on host-guest assembly.

Effective Delivery of RAP by Host-Guest Assemblies for the Treatment of Atherosclerosis

On the basis of above promising findings, additional *in vivo* studies were performed to investigate therapeutic significance of host-guest RAP microspheres for the treatment of atherosclerosis. Also, PLGA and S100 microspheres containing RAP were used as controls. Atherosclerosis was established in ApoE^{-/-} mice by feeding Western diet. After one month, different RAP microparticles were orally administered at 3 mg/kg of RAP every four days for two months, and then animals were sacrificed and aortas were collected from the heart to the iliac bifurcation. The representative *en face* micrographs of ORO-stained aortas directly illuminated the presence of plaques in the whole aorta. Compared with the model control, treatment by either RAP/PLGA or RAP/S100 microspheres failed to effectively attenuate the formation of atherosclerotic lesions (Figure 4A), and statistical analysis revealed no significant difference in the lesion area between the former and the later (Figure 4B). By contrast, therapy with two assembled microspheres of RAP/IND/PNIPAm and RAP/SUL/PNIPAm yielded more desirable outcome. While the area of aortic lesions was 37.3% in the model control, it was decreased to 9.6% and 9.3% after treatment with RAP/IND/PNIPAm and RAP/SUL/PNIPAm microspheres, respectively (Figure 4B). Similar positive results could be found from ORO-stained sections of aortic sinus tissues (Figure 4C-D). In this case, treatment with microspheres of RAP/IND/PNIPAm and RAP/SUL/PNIPAm led to a reduction of 29.7% and 25.7% in the plaque area, respectively. PLGA and S100 microspheres again showed no significant improvement. Therefore, in contrast to RAP-loaded microspheres based on either PLGA or S100, therapy with assembled RAP microspheres could effectively inhibit the formation of atherosclerotic plaques.

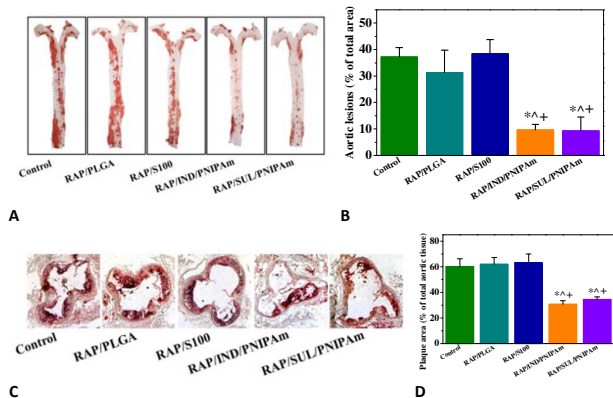


Figure 4. Enhanced oral delivery of RAP resulting in improved atherosclerosis therapy by RAP assemblies in ApoE^{-/-} mice. **A-B.** Representative photographs of ORO-stained aortas (A) and the corresponding quantification (B). **C-D.** Typical cryosections (C) of aortic roots from ApoE^{-/-} mice post treatment and related quantification (D) of lesion areas. Data are mean \pm S.D. (n = 4). *p < 0.01 versus the model control; ^p < 0.01 versus the RAP/PLGA group; and ^p < 0.01 versus the RAP/S100 group.

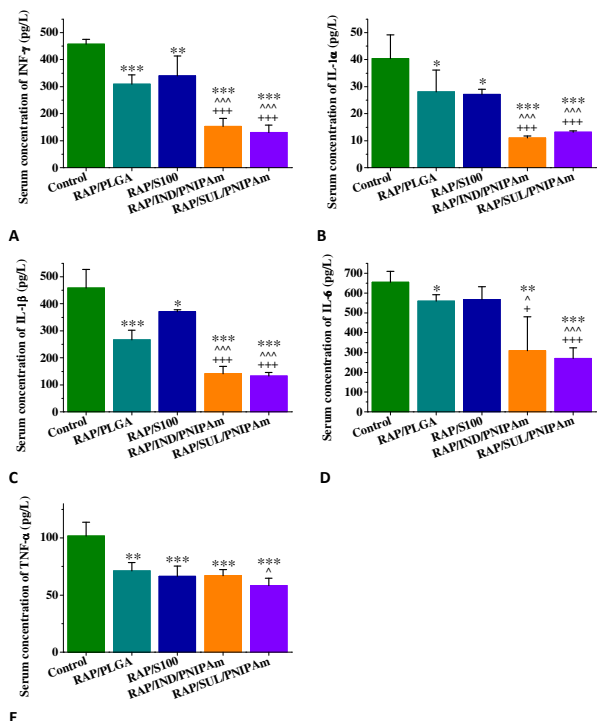


Figure 5. Typical inflammatory cytokines in the serum from ApoE^{-/-} mice subjected to various treatments. Data are mean \pm S.D. (n = 5). INF- γ , interferon- γ ; IL-1 α , interleukin-1 α ; IL-1 β , interleukin-1 β ; IL-6, interleukin-6; and TNF- α , tumor necrosis factor- α . *p < 0.05, **p < 0.01, and ***p < 0.001 versus the model control; ^p < 0.05, ^^p < 0.01, and ^^p < 0.001 versus the RAP/PLGA group; ^p < 0.05, **p < 0.01, and ***p < 0.001 versus the RAP/S100 group.

It has been well demonstrated that inflammatory cytokines are intimately related to the pathogenesis of atherosclerosis, and their higher levels generally indicate the development and progression of atherosclerosis.^{1, 4, 42} Reduced inflammatory cytokines are beneficial for the prevention and treatment of atherosclerotic diseases.^{7, 43} In agreement with the inhibited plaque formation, treatment by RAP assemblies significantly lowered the levels of typical serum inflammatory cytokines like interferon- γ (INF- γ), interleukin-1 α (IL-1 α), interleukin-1 β (IL-1 β), interleukin-6 (IL-6), and tumor necrosis factor- α (TNF- α) (Figure 5). Accordingly, these results unambiguously evidenced that RAP assemblies efficiently mitigated the progression of atherosclerosis, whereas RAP/PLGA and RAP/S100 microspheres could not delay its development. Because atherosclerosis is a complex multifocal arterial disease, to achieve desirable efficacy, drug molecules must reach atherosclerotic lesions that are randomly distributed in the arterial wall. Accordingly, for both PLGA and S100 microspheres, RAP concentrations in the atherosclerotic plaques should be below the minimal effective level that is required to afford significant therapeutic outcome. This was resulted from their low oral bioavailability as substantiated by pharmacokinetic studies (Figure 2E-F).

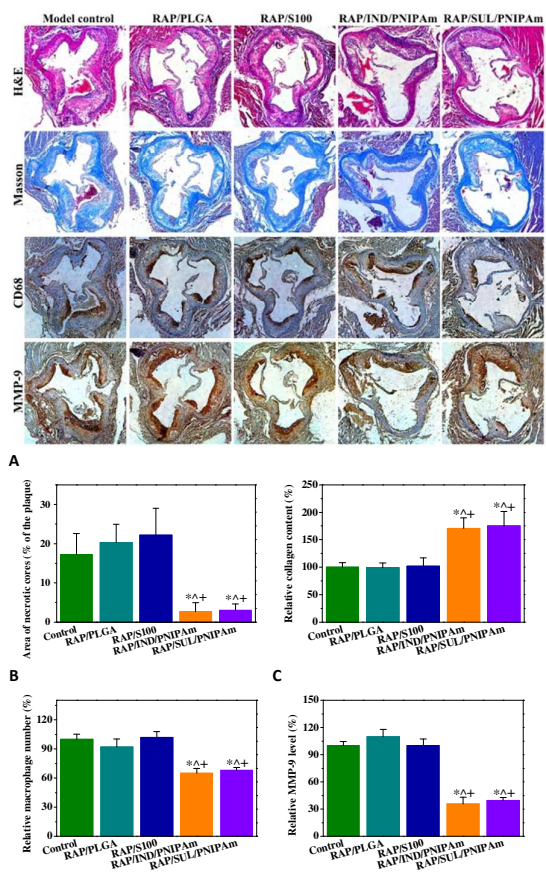


Figure 6. Improved therapy of atherosclerosis by orally delivered RAP via assembled microspheres in ApoE^{-/-} mice. **A**, H&E and immunohistochemistry analyses on cross-sections of aortic roots. **B-E**, Quantitative results of the area of necrotic cores (B), collagen (C), macrophage (D), and MMP-9 (E). Data are mean \pm S.D. (n = 4). *p < 0.01 versus the model control; [#]p < 0.01 versus the RAP/PLGA group; and [^]p < 0.01 versus the RAP/S100 group.

More details regarding the composition of atherosclerotic plaques were provided by histopathological and immunohistochemistry analyses. Examination on H&E stained sections of aortic roots revealed that the necrotic area was dramatically decreased in both RAP/IND/PNIPAm and RAP/SUL/PNIPAm groups (the first row in Figure 6A, Figure 6B). Masson's trichrome and anti-CD68 antibody was separately used to stain collagen and macrophage, while anti-MMP-9 antibody was employed to detect MMP-9. Whereas no distinguishable changes appeared after therapy with PLGA and S100-based RAP microspheres, treatment by RAP assemblies caused evidently increased collagen around plaques as well as significantly decreased macrophage and MMP-9 (the second to fourth rows of Figure 6A, Figure 6C-E). As well demonstrated, increase in the area of necrotic cores, macrophage, and MMP-9 is intimately related to vulnerable plaques, while increased collagen around plaques and therefore the thicker fibrous cap may positively contribute to the plaque stability.⁴⁴ As a result, assembled RAP therapeutics were able to enhance the plaque stability, and inhibit the formation of vulnerable, rupture-prone lesions that may cause many life-threatening atherosclerotic complications. Taken together,

assembled RAP microspheres could efficaciously attenuate the development of atherosclerosis, and effectively delay its progression to more advanced and vulnerable stages.

Also, possible side effects were examined by monitoring changes in the body weight and quantifying the levels of typical lipids such as total cholesterol, low-density lipoprotein (LDL), and high-density lipoprotein (HDL). During and after treatment, we did not find significant weight loss or abnormally varied organ index in all RAP-treated groups as compared to the model control (Figure 7A-B). Moreover, the determined typical lipids showed no remarkable changes in various groups (Figure S4). Besides the significantly increased AST level in the RAP/S100 group, typical hematological parameters and biochemical markers relevant to liver and kidney functions were not notably varied in other groups (Figure 7C-H). Examination on H&E sections indicated that the long-term treatment with assembled RAP therapeutics did not cause discernable injuries in main organs such as heart, liver, spleen, lung, and kidney (Figure 7I). These results suggested that RAP assemblies may not confer adverse effects even after treatment for a long period of time. Therefore PNIPAm assembled delivery systems are safe vehicles for therapeutics against chronic diseases.

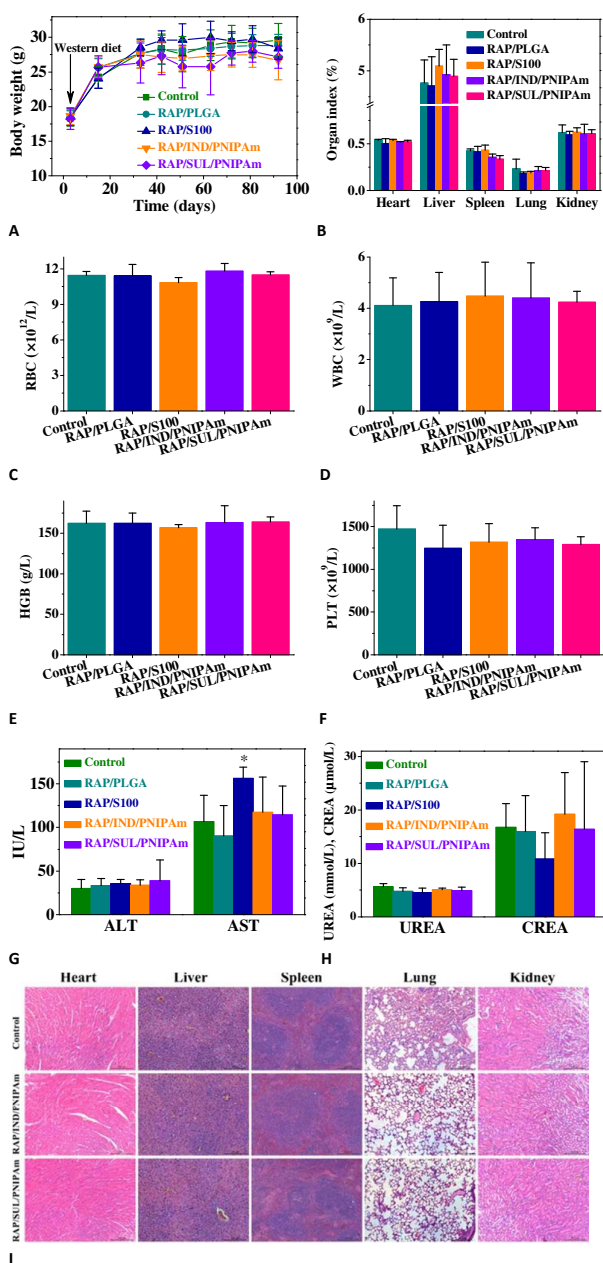


Figure 7. Evaluation of potential side effects in ApoE^{-/-} mice during and after treatment with different RAP microspheres. **A**, Changes in the body weight of mice during the long-term treatment. Data are mean \pm S.D. (n = 10). **B**, The organ index. Data are mean \pm S.D. (n = 10). **C-F**, Hematological parameters. RBC, red blood cell; WBC, white blood cell; HGB, hemoglobin; and PLT, platelet. Data are mean \pm S.D. (n = 6). **G-H**, Levels of biochemical markers relevant to liver (G) and kidney (H) functions. Data are mean \pm S.D. (n = 6). *p < 0.01 versus the model control. **I**, H&E stained sections of main organs collected post therapy.

In Vivo Chronic Toxicity Evaluation of PNIPAm for Oral Delivery

Whereas PNIPAm and its copolymers have been broadly investigated for biomedical applications such as drug delivery and tissue regeneration,⁴⁵⁻⁴⁸ their *in vivo* safety profiles remain to be elucidated. Since our results revealed the great potential of PNIPAm-based therapeutic assemblies for oral drug delivery, herein we conducted preliminary evaluation in mice to explore *in vivo* safety of PNIPAm. PNIPAm was administered by gastric gavage once every four days at doses varying from 125, 250, 500, to 1000 mg/kg for six months. During this long period of treatment time, no any alterations in behaviour, food intake, body weight, and body temperature were found for animals treated with PNIPAm, irrespective of various doses administered. We could observe gradual gains in the animal body weight, without statistical differences between the control and PNIPAm-treated groups (Figure 8A). After treatment, the blood and major organs were collected. Quantification of biomarkers including ALT, AST, UREA, and CREA showed no significant variations as compared to the saline group (Figure 8B-C). Besides, the serum levels of typical lipids such as TCH, TG, HDL, and LDL were not evidently varied (Figure 8D). Likewise, complete blood count indicated comparable numbers of WBC, RBC, and PLT as well as HGB concentration (Figure 8E).

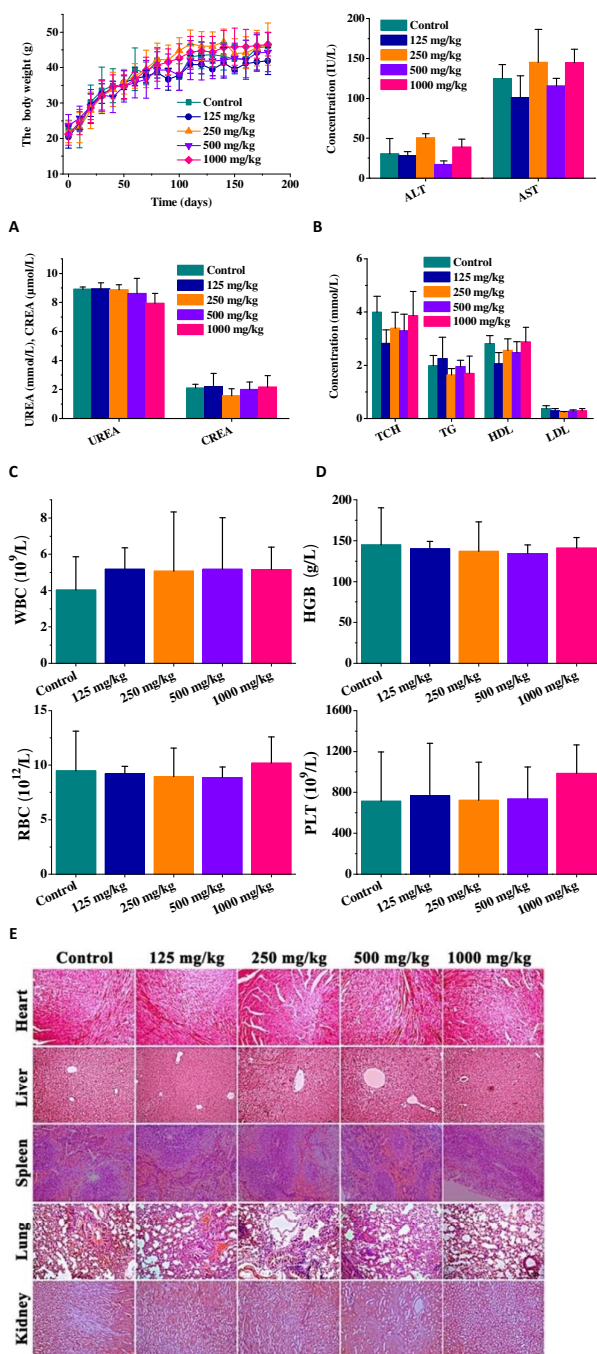


Figure 8. Toxicological evaluation of PNIPAm after long-term oral administration in mice. **A**, Changes in the body weight of mice treated with PNIPAm at various doses. **B–C**, Biochemical markers relevant to liver (**B**) and kidney (**C**) functions. **D**, Quantification of blood lipids. TCH, total cholesterol; TG, triglyceride; LDL, low-density lipoprotein; HDL, high-density lipoprotein. **E**, Hematological parameters of blood samples from mice subjected to various treatments. **F**, Histopathological sections of major organs resected from mice continuously treated with normal saline or PNIPAm for 180 days. Data are as mean \pm S.D. ($n = 10$). * $p < 0.05$ compared with the saline control. Images were taken at $\times 10$ magnification with standard H&E staining.

Moreover, inspection on H&E sections implied no significant pathological changes in various major organs (including heart, liver, spleen, lung, and kidney) for different PNIPAm groups (Figure 8F). According to the drug loading capacity of PNIPAm assemblies, it is worth noting that the dose of 1000 mg/kg of PNIPAm is about 500 times higher than that of the practically used dose when it is utilized *in vivo* for RAP delivery. Overall, these preliminary findings demonstrated that PNIPAm may serve as a safe material for oral drug delivery, although more convincing data should be provided by good laboratory practice (GLP) based non-clinical safety tests in different animals.

Conclusions

In summary, we found that an anti-atherosclerotic drug RAP can be effectively loaded into microspheres by a host-guest assembly approach, using a structurally simple host polymer of PNIPAm. This strategy afforded cost-effective therapeutic assemblies with particularly robust drug loading capacity, desirable drug release profiles, good lyophilization-reconstitution character, and facile scalability. Besides these superior pharmaceutical characteristics over the emulsion method-based PLGA and S100 microspheres, RAP assemblies fabricated by this approach displayed high oral bioavailability. More importantly, assembled RAP microspheres displayed significantly potentiated efficacy for the treatment of atherosclerosis. Additionally, long-term treatment with either RAP-containing assemblies or the carrier material of PNIPAm revealed good safety performance post oral administration in mice. Consequently, RAP assemblies developed herein are promising therapeutics for the management of atherosclerotic diseases, immune rejection after transplantation, aging and age-related disease, and other chronic diseases as well as for the life-span extension. Moreover, this study provides new insights into the design of effective carrier materials for a diverse array of lipophilic therapeutics.

Acknowledgements

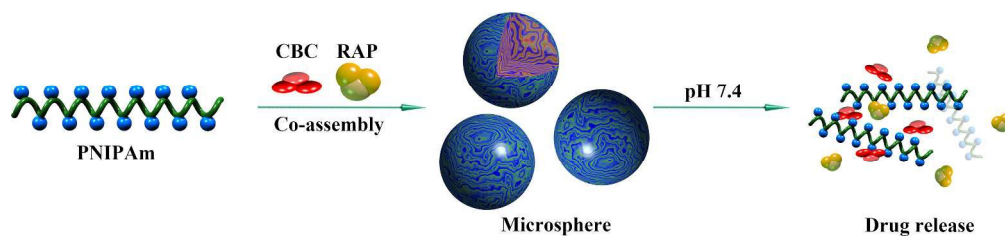
We gratefully acknowledge financial support by the National Natural Science Foundation of China (No. 81271695 & 81471774) and the Research Foundation of Third Military Medical University (2014XJY04). This study was also supported by Program for New Century Excellent Talents in University (NCET-13-0703) to JXZ.

Notes and references

^aDepartment of Pharmaceutics, College of Pharmacy, Third Military Medical University, Chongqing 400038, China. E-mail: jxzhang1980@gmail.com; jxzhang@tmmu.edu.cn; sumin@yahoo.cn.
^bInstitute of Materia Medica, College of Pharmacy, Third Military Medical University, Chongqing 400038, China. E-mail: lpsh008@aliyun.com.

1. G. K. Hansson, *N. Engl. J. Med.*, 2005, **352**, 1685-1695.
2. E. G. Nabel and E. Braunwald, *N. Engl. J. Med.*, 2012, **366**, 54-63.

3. F. K. Swirski and M. Nahrendorf, *Science*, 2013, **339**, 161-166.
4. P. Libby, *Nature*, 2002, **420**, 868-874.
5. P. Libby, P. M. Ridker and G. K. Hansson, *Nature*, 2011, **473**, 317-325.
6. I. Tabas and C. K. Glass, *Science*, 2013, **339**, 166-172.
7. I. F. Charo and R. Taub, *Nat. Rev. Drug Discov.*, 2011, **10**, 365-376.
8. P. Linsel-Nitschke and A. R. Tall, *Nat. Rev. Drug Discov.*, 2005, **4**, 193-205.
9. J. W. Moses, M. B. Leon, J. J. Popma, P. J. Fitzgerald, D. R. Holmes, C. O'Shaughnessy, R. P. Caputo, D. J. Kereiakes, D. O. Williams, P. S. Teirstein, J. L. Jaeger and R. E. Kuntz, *N. Engl. J. Med.*, 2003, **349**, 1315-1323.
10. L. O. Jensen, P. Thayssen, H. S. Hansen, E. H. Christiansen, H. H. Tilsted, L. R. Krusell, A. B. Villadsen, A. Junker, K. N. Hansen, A. Kaltoft, M. Maeng, K. E. Pedersen, S. D. Kristensen, H. E. Botker, J. Ravkilde, R. Sanchez, J. Aaroe, M. Madsen, H. T. Sorensen, L. Thuesen and J. F. Lassen, *Circulation*, 2012, **125**, 1246-1255.
11. L. Zhao, T. Ding, T. Cyrus, Y. Cheng, H. Tian, M. Ma, R. Falotico and D. Praticò, *Brit. J. Pharmacol.*, 2009, **156**, 774-785.
12. C. Castro, J. M. Campistol, D. Sancho, F. Sanchez-Madrid, E. Casals and V. Andres, *Atherosclerosis*, 2004, **172**, 31-38.
13. M. Poon, S. O. Marx, R. Gallo, J. J. Badimon, M. B. Taubman and A. R. Marks, *J. Clin. Invest.*, 1996, **98**, 2277-2283.
14. W. Martinet and G. R. Y. De Meyer, *Circ. Res.*, 2009, **104**, 304-317.
15. M. Laplante and D. M. Sabatini, *Cell*, 2012, **149**, 274-293.
16. C. Y. Wu and L. Z. Benet, *Pharm. Res.*, 2005, **22**, 11-23.
17. P. Simamora, J. M. Alvarez and S. H. Yalkowsky, *Int. J. Pharm.*, 2001, **213**, 25-29.
18. R. W. Yatscoff, *Transplant. Proc.*, 1996, **28**, 970-973.
19. J. X. Zhang, K. Ellsworth and P. X. Ma, *J. Control. Release*, 2010, **145**, 116-123.
20. M. A. Rouf, E. Bilensoy, I. Vural and A. A. Hincal, *Eur. J. Pharm. Sci.*, 2007, **32**, S46-S47.
21. W. Dai, F. Yang, L. Ma, Y. Fan, B. He, Q. He, X. Wang, H. Zhang and Q. Zhang, *Biomaterials*, 2014, **35**, 5347-5358.
22. M. L. T. Zweers, G. H. M. Engbers, D. W. Grijpma and J. Feijen, *J. Control. Release*, 2006, **114**, 317-324.
23. J. X. Zhang, Y. Jia, X. D. Li, Y. Q. Hu and X. H. Li, *Adv. Mater.*, 2011, **23**, 3035-3040.
24. X. Zhou, L. Che, Y. L. Wei, Y. Dou, S. Chen, H. M. He, H. Gong, X. H. Li and J. X. Zhang, *Acta Biomater.*, 2014, **10**, 2630-2642.
25. M. L. Forrest, C. Y. Won, A. W. Malick and G. S. Kwon, *J. Control. Release*, 2006, **110**, 370-377.
26. S. Khondee, E. F. Rabinsky, S. R. Owens, B. P. Joshi, Z. Qiu, X. Duan, L. Zhao and T. D. Wang, *J. Control. Release*, 2015, **199**, 114-121.
27. S. Jhunjhunwala, G. Raimondi, A. W. Thomson and S. R. Little, *J. Control. Release*, 2009, **133**, 191-197.
28. L. L. Falke, S. H. van Vuuren, F. Kazazi-Hyseni, F. Ramazani, T. Q. Nguyen, G. J. Veldhuis, E. M. Maarseveen, J. Zandstra, J. Zuidema, L. F. Duque, R. Steendam, E. R. Popa, R. J. Kok and R. Goldschmeding, *Biomaterials*, 2015, **42**, 151-160.
29. W. Tai, Z. Chen, A. Barve, Z. Peng and K. Cheng, *Pharm. Res.*, 2014, **31**, 706-719.
30. E. M. Pridgen, F. Alexis, T. T. Kuo, E. Levy-Nissenbaum, R. Karnik, R. S. Blumberg, R. Langer and O. C. Farokhzad, *Sci. Transl. Med.*, 2013, **5**, 213ra167.
31. J. X. Zhang, K. Feng, M. Cuddihy, N. A. Kotov and P. X. Ma, *Soft Matter*, 2010, **6**, 610-617.
32. A. D. Costache, L. Sheihet, K. Zaveri, D. D. Knight and J. Kohn, *Mol. Pharmaceutics*, 2009, **6**, 1620-1627.
33. G. M. Morris, R. Huey, W. Lindstrom, M. F. Sanner, R. K. Belew, D. S. Goodsell and A. J. Olson, *J. Comput. Chem.*, 2009, **30**, 2785-2791.
34. J. X. Zhang, D. Chen, S. J. Wang and K. J. Zhu, *J. Microencapsul.*, 2005, **22**, 413-422.
35. C. Wischke and S. P. Schwendeman, *Int. J. Pharm.*, 2008, **364**, 298-327.
36. M. Li, O. Rouaud and D. Poncelet, *Int. J. Pharm.*, 2008, **363**, 26-39.
37. Y. X. Zhu, L. Che, H. M. He, Y. Jia, J. X. Zhang and X. H. Li, *J. Control. Release*, 2011, **152**, 317-324.
38. X. Zhou, S. L. Han, Q. X. Zhang, Y. Dou, J. W. Guo, L. Che, X. H. Li and J. X. Zhang, *Polym. Chem.*, 2015, **6**, 3716-3727.
39. Y. Dou, Y. Jia, X. Zhou, J. X. Zhang and X. H. Li, *Cryst. Growth Des.*, 2011, **11**, 899-904.
40. S. R. Vippagunta, H. G. Brittain and D. J. Grant, *Adv. Drug Deliv. Rev.*, 2001, **48**, 3-26.
41. J. X. Zhang, S. H. Li, X. H. Li, L. Y. Qiu, X. D. Li, X. J. Li, Y. Jin and K. J. Zhu, *J. Biomed. Mater. Res. A*, 2008, **86A**, 914-925.
42. E. Galkina and K. Ley, *Annu. Rev. Immunol.*, 2009, **27**, 165-197.
43. R. Klingenberg and G. K. Hansson, *Eur. Heart J.*, 2009, **30**, 2838-2844.
44. M. Naghavi, P. Libby, E. Falk, S. W. Casscells, S. Litovsky, J. Rumberger, J. J. Badimon, C. Stefanadis, P. Moreno, G. Pasterkamp, Z. Fayad, P. H. Stone, S. Waxman, P. Raggi, M. Madjid, A. Zarrabi, A. Burke, C. Yuan, P. J. Fitzgerald, D. S. Siscovick, C. L. de Korte, M. Aikawa, K. E. J. Airaksinen, G. Assmann, C. R. Becker, J. H. Chesebro, A. Farb, Z. S. Galis, C. Jackson, I. K. Jang, W. Koenig, R. A. Lodder, K. March, J. Demirovic, M. Navab, S. G. Priori, M. D. Rekhter, R. Bahr, S. M. Grundy, R. Mehran, A. Colombo, E. Boerwinkle, C. Ballantyne, W. Insull, R. S. Schwartz, R. Vogel, P. W. Serruys, G. K. Hansson, D. P. Faxon, S. Kaul, H. Drexler, P. Greenland, J. E. Muller, R. Virmani, P. M. Ridker, D. P. Zipes, P. K. Shah and J. T. Willerson, *Circulation*, 2003, **108**, 1664-1672.
45. S. Mura, J. Nicolas and P. Couvreur, *Nat. Mater.*, 2013, **12**, 991-1003.
46. J. X. Zhang, X. D. Li and X. H. Li, *Prog. Polym. Sci.*, 2012, **37**, 1130-1176.
47. A. K. A. S. Brun-Graeppe, C. Richard, M. Bessodes, D. Scherman and O. W. Merten, *Prog. Polym. Sci.*, 2010, **35**, 1311-1324.
48. H. Wei, S. X. Cheng, X. Z. Zhang and R. X. Zhuo, *Prog. Polym. Sci.*, 2009, **34**, 893-910.



1255x280mm (72 x 72 DPI)